On the Modeling of New Tunnel Junction Magnetoresistive Biosensors

Teresa Mendes de Almeida, Moisés S. Piedade, Leonel Augusto Sousa, *Senior Member, IEEE*, José Germano, Paulo A. C. Lopes, Filipe Arroyo Cardoso, and Paulo Peixeiro Freitas, *Member, IEEE*

***Abstract*—A fully integrated biochip based on a 16 × 16 scalable matrix structure of aluminum oxide magnetic tunnel junctions (MTJs) and thin-film diodes (TFDs of hydrogenated amorphous silicon) was fabricated and included as the biosensor of a portable handheld microsystem developed for biomolecular recognition detection using magnetic labels [deoxyribonucleic acid (DNA) hybridization, antibody antigen interaction, etc.]. The system uses magnetic field arraying of magnetically tagged biomolecules and can potentially be used to detect single or few biomolecules. Each biosensor matrix node is the series between a TFD (p-i-n or Schottky-barrier type) and an MTJ. In this paper, this matrix basic cell biosensor element is completely characterized and modeled. Experimental measured data are provided and compared with the proposed theoretical models results. It is shown that the diode may be used both as the matrix switching device and as an in-site temperature sensor and that the MTJ may act as the magnetoresistive sensor for detecting the fringe field of immobilized magnetic markers. Therefore, the fabricated fully integrated biochip included in the developed handheld microsystem may be used for biomolecular recognition.**

***Index Terms*—Biomedical transducers, magnetoresistive devices, p-i-n diodes, Schottky diodes, system modeling.**

I. Introduction

NOWADAYS, magnetoresistive biochips are considered for fully integrated biomolecular recognition assays using target biomolecules marked with magnetic particles [1]. Labeled target biomolecules are recognized by biomolecular probes immobilized on the surface of the chip over the sensing sites. Among the various types of magnetic sensors [i.e., giant magnetoresistive sensors, spin valve resistors, and magnetic tunnel junctions (MTJs)], MTJs assume great importance. This is due to their greater flexibility in resistance design and higher magnetic sensitivity and because they benefit from recent research and technological advances aimed at the design of future ultra-high-density magnetic memory chips. Furthermore, when compared with other types of magnetic sensors, MTJs enable the detection of smaller magnetic labels [2].

Manuscript received February 11, 2008; revised April 14, 2009. First published November 10, 2009; current version published December 9, 2009. The Associate Editor coordinating the review process for this paper was Dr. Subhas Mukhopadhyay.

T. M. de Almeida, M. S. Piedade, L. A. Sousa, and P. A. C. Lopes are with the Instituto de Engenharia de Sistemas e Computadores-R&D (INESC-ID), Lisbon 1000-029, Portugal, and also with Instituto Superior Técnico, Technical University of Lisbon, Lisbon 1000-029, Portugal (e-mail: Teresa.Almeida@inesc-id.pt).

J. Germano is with the INESC-ID, Lisbon 1000-029, Portugal.

F. A. Cardoso is with the Instituto de Engenharia de Sistemas e Computadores-Microsistemas and Nanotecnologias (INESC-MN), Lisbon 1000-029, Portugal.

P. P. Freitas is with the INESC-MN, Lisbon 1000-029, Portugal, and also with the Instituto Superior Técnico, Technical University of Lisbon, Lisbon 1000-029, Portugal.

Color versions of one or more of the figures in this paper are available online at http://ieeexplore.ieee.org.

Digital Object Identifier 10.1109/TIM.2009.2022100

A. Handheld Microsystem

The magnetoresistive biosensor that is characterized and modeled in this paper is the basic cell at each site of a 16 × 16 matrix structure in a fully integrated biochip that is included on a compact (credit card dimension) and portable handheld microsystem for biomolecular recognition usage [3], [4]. The microsystem integrates the biochip and provides all the electronic circuitry for addressing, reading out, sensing, temperature controlling, and fluid sample handling. Readout signals are processed through advanced signal processing techniques implemented on a digital signal processor (DSP). In addition to signal processing, the DSP reduces noise and offset effects and controls biochip temperature and the analog circuitry. High-level system control and data analysis are remotely performed through a personal digital assistant via a wireless channel or a universal serial bus. A prototype has already been developed, and the experimental results show that it may be used for magnetically labeled target biomolecule detection [3]–[5].

B. Biochip Structure

The magnetoresistive biochip [fabricated at the Instituto de Engenharia de Sistemas e Computadores-Microsistemas and Nanotecnologias (INESC-MN) using standard microfabrication techniques] has 256 biosensor detection sites (16 × 16 matrix). Each magnetoresistive biosensor basic element consists of a thin-film diode (TFD) in series with an MTJ [6], [7]. From the technology available at INESC-MN, the following two types of hydrogenated amorphous silicon (a-Si:H) TFDs are considered: 1) p-i-n diode (p-n semiconductor junction diode with an intrinsic layer between the p and n regions—here abbreviated as PIN diode) and 2) Schottky-barrier diode (same technology as in [8], although a different biochip with distinct features is considered).

Each diode has the following two main functions: 1) It acts as a switching device enabling matrix column–row selection allowing a unique current path (in a similar way as it happens in memory structures row–column connections) and 2) it acts as a temperature sensor of each biosensor site. Each MTJ $(10 \times 2\ \mu\text{m}^2)$ is very close (only 34 μm apart) to the

associated TFD ($200 \times 200\ \mu m^2$) and operates as a sensor of the planar magnetic field transversal to its length [4]. The TFD is not affected by the magnetic field, but the MTJ has a small temperature dependence that is negligible when compared to the TFD temperature sensitivity, as will be shown later in this paper.

Biochip biosensor characterization and modeling is fundamental to sense local temperature, perform temperature control, and achieve system calibration. In the following, biochip magnetoresistive biosensors are characterized, and theoretical models describing their behavior are proposed.

This paper is organized as follows. Section II describes a model for the biosensor element driven by a measuring current and a small-signal model that enables temperature and magnetic sensitivity determination. Sections III–VI address TFD electrical and temperature modeling and characterization. Section VII focuses on MTJ electrical, temperature, and magnetic modeling and characterization. Finally, Section VIII provides conclusions.

II. Biosensor Modeling

Biomolecular recognition is performed through magnetic labels detection. The labeled target biomolecules are recognized by biomolecular probes immobilized over the sensing sites. Considering, for example, the biosensor usage for deoxyribonucleic acid (DNA) hybridization detection, the target DNA, tagged with paramagnetic nanoparticles, is transported in a fluid and is focused at sensing sites using alternating magnetic field gradients. The target DNA hybridizes with available complementary probes, and magnetic labels remain bound to the surface of the sensors after chip washing with a buffer solution [4]. An external magnetic field induces a magnetic moment on the nanospheres, and each MTJ sensor will detect this change proportionally to the number of labels bound to its surface. The reading of each biosensor matrix element is performed through a set of ac and dc current drive techniques to measure site temperature T and the local change ΔH of the external magnetic field H originated by the hybridization of magnetically labeled target DNAs to the probes. The dc current path goes through a unique selected biosensor basic cell (a unique matrix node), polarizes the TFD, and establishes an MTJ operating point with low impedance. It is this dc component of the current that permits the TFD to sense local temperature. On the other hand, an ac current component is necessary because the main objective is to measure a magnetic field variation through the corresponding MTJ resistance variation. Isolation between ac and dc current components is achieved via high-pass filtering, which permits ac signal amplification of about 1000 times at a subsequent processing stage [3].

When each basic biosensor element (each matrix node) is driven with a measuring current i_M, small changes on the MTJ resistance due to magnetic field variations are read as small voltage changes at the input driving port. Each biosensor element (TFD in series with the MTJ) may then be characterized by a current-driven model (Fig. 1). The diode is susceptible to absolute temperature T and may present some sensitivity to incident light L (see Section III), while the magnetoresistance

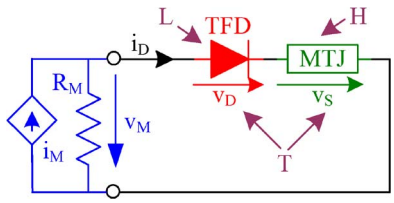

Fig. 1. Current driven biosensor element model (H: external magnetic field; T: absolute temperature; and L: incident light).

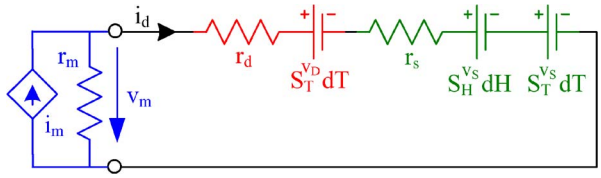

Fig. 2. Biosensor element small-signal model.

is responsive to the magnetic field H and only slightly sensitive to temperature (see Section VII).

In a complete model, taking into account all three external stimulus (i.e., H, T, and L), the biosensor measured voltage v_M has a nonlinear relationship with the measuring current i_M ($i_M \approx i_D$ for high R_M), the external magnetic field, site absolute temperature, and incident light throughout the TFD and MTJ developed voltages (v_D and v_S, respectively), i.e.,

$$v_M = v_D(i_M, T, i_L) + v_S(i_M, T, H) \tag{1}$$

where i_L represents a contribution due to the photovoltaic effect whenever this effect is present. If this is not the case or if its influence is negligible, v_D only depends on the measuring current and absolute temperature contributions ($v_D(i_M, T)$).

When the photovoltaic effect is not present, a small variation on the biosensor voltage $dv_M = v_m$, resulting from small changes or perturbations in the main variables, namely, $di_M = i_m$, dT, or dH, may be characterized via a small-signal model (Fig. 2), which is valid near a quiescent point (I_M, T, H), i.e.,

$$dv_M = (r_d + r_s)di_M + \left(S_T^{v_D} + S_T^{v_S}\right)dT + S_H^{v_S}dH \tag{2}$$

with $r_d = S_{i_M}^{v_D} = \partial v_D/\partial i_M$ and $r_s = S_{i_M}^{v_S} = \partial v_S/\partial i_M$. The main objective is then to be able to measure the external magnetic field variations through the MTJ sensitivity (i.e., $S_H^{v_S} = S_H^{R_S} i_M$) at constant I_M and T as well as temperature variations via the TFD sensitivity (i.e., $S_T^{v_D} \gg S_T^{v_S}$ as shown in the next sections). Biosensor characteristics and quiescent operating points assure a low contribution due to the first term, i.e., $(r_d + r_s)di_M$, through low-enough incremental resistance values (i.e., r_d and r_s).

The next sections describe TFD and MTJ characterization and modeling, and their sensitivities $(r_d, S_T^{v_D})$ and $(r_s, S_H^{v_S}, S_T^{v_S})$ are analyzed according to this proposed biosensor model and the specific developed biosensor models.

III. TFD Characterization and Modeling

The following two TFDs were considered for matrix addressing and temperature sensing: 1) a Schottky-barrier diode, which

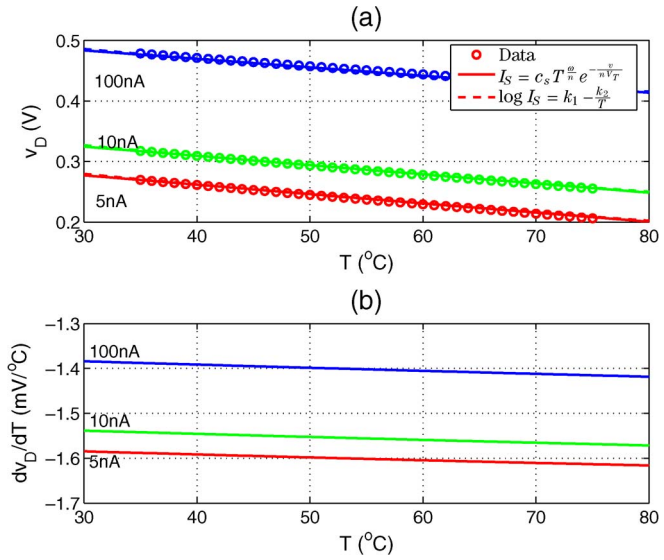

Fig. 3. Schottky-barrier diode temperature dependence at low currents. (a) $v_D(T, I_D)$ (circle marks: experimental data; solid and dashed lines: proposed models). (b) $S_T^{v_D}(T, I_D)$ obtained with the proposed biosensor models.

has an almost linear temperature sensitivity [see Fig. 3(b)], and 2) a PIN diode, which supports higher currents, acts more quickly, and has higher temperature sensitivities but a less linear characteristic (see Fig. 7). TFD modeling is accomplished starting from a low-current region (LCR) model, moving to a medium-current region (MCR), in the case of the PIN diode, and finally, a complete compound model is obtained for the high-current region (HCR).

IV. Schottky-Barrier Diode Modeling

A. Schottky Diode at Low Currents

In the LCR, the Schottky-barrier diode behavior may be characterized by the following Schockley equation [9] of a crystalline semiconductor junction:

$$v_D = v_J = nV_T \ln(1 + i_D/I_S). \tag{3}$$

Although all parameters are temperature dependent (i.e., n, the emission coefficient, $V_T = KT/q$, the thermal voltage, and I_S, the diode saturation current), only V_T temperature dependency is known. To use the TFD as a temperature sensor characterized by $S_T^{v_D}$, it is necessary to know how $n(T)$ and $I_S(T)$ depend on temperature. For three small current values, i.e., 5, 10, and 100 nA, the TFD response to temperature was measured through $v_D(T)$ registration while temperature was decreasing. Current was held constant and $v_D(T)$ values were digitally acquired while the biochip was held inside an enclosed heated compartment, and a high temperature value (≈80 °C) was initially set. Temperature decreased for about 2 h until a constant temperature value was reached inside the stove. Biochip temperature values were experimentally determined using a thermocouple (standard type K) attached to the biochip and acquiring and registering its voltage. Circle marks in Fig. 3(a) correspond to obtained experimental data and suggest an almost linear $v_D(T)$ variation for the three current values.

From the set of experimentally measured $v_D(T)$, values of $n(T)$ were determined for each T, and $I_S(T)$ was then calculated using the obtained $(v_D(T), n(T))$ pairs (see (3) in reference [6]). From this set of experiments, $S_T^{v_D}$ has been completely characterized for small currents values.

Experimental data obtained for $n(T)$ and $I_S(T)$ lead to the following models [6], [10]:

$$n(T) = n_1 + n_2/T \tag{4}$$

$$\log\left[1/I_S(T)\right] = k_1 + k_2/T \tag{5}$$

with coefficients $n_1 = 7.8186 \times 10^{-1}$, $n_2 = 5.6641 \times 10^2$, $k_1 = 6.0608$, and $k_2 = 1.2085 \times 10^3$ directly estimated from the experimental data. Accordingly to the obtained model, $n(T)$ has a variation of about -10% in a 50 °C range (30 °C–80 °C) [6].

To technologically characterize the diode, another model was considered [4] with the purpose of taking into account technologic junction parameters [i.e., c_S, n, ω, and v in (6)] and the fact that I_S has a temperature dependence, which is a function of the square of intrinsic carriers concentration (which increases strongly with T) [11], i.e.,

$$I_S(T) = c_S T^{\frac{\omega}{n}} e^{-\frac{v}{nV_T}} \tag{6}$$

where it is assumed that $n(T)$ temperature dependence is modeled by (4) (with the estimated coefficients), but that the remaining parameters, namely, c_S, ω, and v, are constants and do not depend on temperature. From experimental data and the proposed models, $c_S = 1.2671 \times 10^{-8}$, $\omega = 2.6327$, and $v = 7.3333 \times 10^{-1}$ V were obtained [6]. Solid (model with technological parameters) and dashed (model with k_1 and k_2) lines in Fig. 3(a) confront experimental data (circle marks) with the two proposed models. The accordance between results for both models and experimental data show that $n(T)$ model and both $I_S(T)$ models may be considered for the TFD temperature dependence in the LCR.

When (5) is considered for $I_S(T)$, the I_S temperature coefficient (fractional change in I_S per unit change in T) is

$$\frac{1}{I_S}\frac{dI_S}{dT} = \frac{1}{I_S} S_T^{I_S} = \ln 10 \frac{k_2}{T^2} \tag{7}$$

and 30 °C, 50 °C, and 80 °C variations of 3%/°C, 2.7%/°C, and 2.2%/°C are, respectively, obtained.

When the model with technological parameters [see (6)] is considered, the temperature coefficient is

$$\frac{1}{I_S}\frac{dI_S}{dT} = \frac{1}{I_S} S_T^{I_S} = \frac{1}{nT}\left[\frac{n_1}{n}\frac{v}{V_T} + w\left(1 + \frac{n_2}{n}\frac{\ln T}{T}\right)\right] \tag{8}$$

and variations of 2.7%/°C, 2.6%/°C, and 2.5%/°C are obtained for 30 °C, 50 °C, and 80 °C, respectively.

It can then be said that at room temperature, a variation of about 3%/°C may be expected for I_S with both models (a variation of about 23 °C is needed for the current to double its value), which is a lower value than what is usually considered for a silicon p-n junction diode, i.e., 15%/°C (current doubles for each 5 °C variation) [11].

Commonly, at $I_D = 1$ mA, the measured $S_T^{v_J}$ for a p-n junction silicon diode is set to around -2 mV/°C [11]. Since experimental data [circle marks in Fig. 3(a)] suggest an almost linear variation for $v_D(T)$ in the LCR, when a simple linear fit over experimental data is considered, an estimated constant temperature sensitivity of $S_T^{v_D} = -1.61$, -1.56, and -1.38 mV/°C is obtained for the considered current values (5, 10, and 100 nA, respectively). The obtained TFD sensitivities are then similar to those of a p-n silicon diode, although forward current values are now much lower.

Considering the proposed models [see (4) and (6)], the TFD $S_T^{v_D}$ at a quiescent point (I_D, V_D, n, T) in the LCR is

$$S_T^{v_D} = \frac{1}{T}\left[\frac{n_1}{n}V_D - \frac{I_D}{I_D + I_S}\left[\frac{n_1}{n}v + \omega V_T\left(1 + \frac{n_2}{n}\frac{\ln T}{T}\right)\right]\right] \tag{9}$$

which, for $i_D \gg I_S$, simplifies to [6]

$$S_T^{v_D} = \frac{1}{T}\left[\frac{n_1}{n}(V_D - v) - \omega V_T\left(1 + \frac{n_2}{n}\frac{\ln T}{T}\right)\right]. \tag{10}$$

For the considered temperature range (i.e., 30 °C−80 °C), $S_T^{v_D}$ corresponds to an almost linear characteristic as depicted in Fig. 3(b) for the three current values. The curves show a good agreement with the anticipated values (previously predicted from a simple direct linear fit over experimental data). Because of its characterized and now modeled temperature sensitivity, each TFD may then be used to sense local temperature values. Due to the biochip fabrication technology and geometry, each TFD is very close and has a very good thermal connection with the corresponding MTJ on each basic cell, which allows it to sense in-site temperature.

B. Schottky Diode at High Currents

The I–V characteristic of the thin-film Schottky-barrier diode is slightly different from the I–V characteristic of a crystalline semiconductor junction due to the space-charge-current-limited phenomenon that typically occurs in amorphous semiconductor films [9], [10]. This phenomenon occurs in the bulk access to the junction and leads to a voltage drop in the bulk region that varies nonlinearly with current.

For high current values, the diode electrical behavior may be modeled as a sum of v_J [see (3)] and the voltage drop over a nonlinear resistor R, i.e.,

$$v_D = v_J + v_\alpha = n\,V_T \ln(1 + i_D/I_S) + (R\,i_D)^\alpha \tag{11}$$

which establishes a compound model valid both in the LCR and in the HCR. This model achieves good results for current values up to ≈ 70 μA, which is the practical upper limit for MTJ proper operation.

To completely characterize the TFD electrical and temperature behavior, experimental data were obtained, measuring $v_D(T)$ at a set of different temperatures both for low and high current imposed values (2 nA–0.1 μA and 0.08–80 μA). Current was held constant for 3 s, and each obtained $v_D(T)$ value corresponds to an average of ten consecutive voltage acquisitions. Experimental results for the TFD I–V measured characteristics are depicted as marks in Fig. 4 for temperatures in the range of 30 °C–80 °C that were set while the TFD was inside an enclosed heated compartment (same apparatus as previously described).

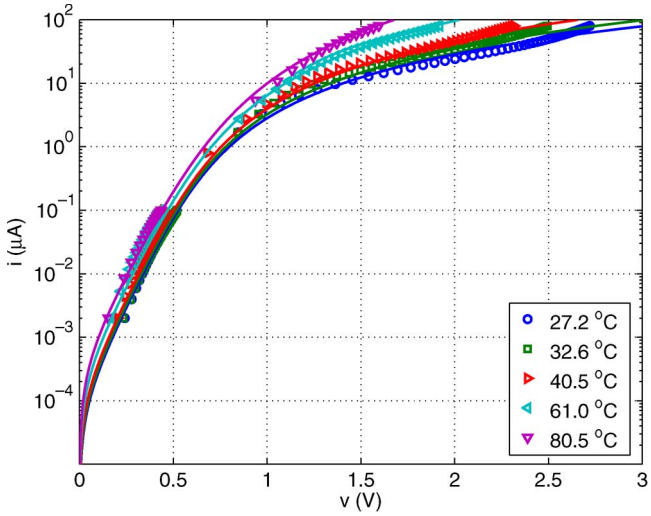

Fig. 4. Schottky-barrier diode I–V characteristics for several temperatures (marks: experimental data; lines: theoretical model).

R and α in (11) also depend on temperature, and the following linear models for $\log[R(T)]$ and $\alpha(T)$ may be considered:

$$\log\left[R(T)\right] = r_1 - r_2 T \quad \alpha(T) = \alpha_1 - \alpha_2 T. \tag{12}$$

From the set of experimental data acquired at different temperatures, coefficients $r_1 = 9.5561$, $r_2 = 1.6407 \times 10^{-2}$, $\alpha_1 = 1.2635$, and $\alpha_2 = 2.2276 \times 10^{-3}$ were obtained [6]. From the derived model, $R \approx 50$ kΩ is expected at room temperature.

Solid lines in Fig. 4 represent the TFD I–V characteristics using the proposed compound model for the same set of temperature values as experimental measures were conducted. It can be seen that a good characterization is obtained for current levels almost until 70 μA. A better characterization is obtained for higher operating temperatures because for lower temperatures and very high currents (> 70 μA), I–V curves deviate and rise superlinearly. Although the considered model characterizes very well the TFD for the current range of the intended application (which is limited by the MTJ maximum allowable current), if a perfect match is desired in the very high current region, the proposed model may be completed with the model of a junction diode in parallel with the junction, and the nonlinear resistance already included.

Due to $R(T)$ and $\alpha(T)$, v_α is also temperature dependent, and its sensitivity at a quiescent point is

$$S_T^{v_\alpha} = -(RI_D)^\alpha\left[r_2\alpha \ln 10 + \alpha_2 \ln(RI_D)\right]. \tag{13}$$

For constant temperature, the $S_T^{v_\alpha}$ magnitude rises with i_D, and, for constant i_D, the $S_T^{v_\alpha}$ magnitude decreases in a nonlinear way as temperature augments. For this reason, the TFD should be used as a temperature sensor only in the LCR where there is no need to consider a compound model.

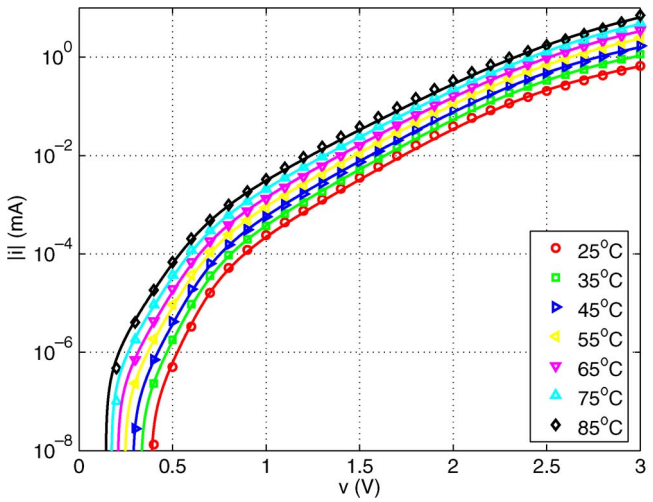

Fig. 5. PIN diode I–V characteristics for several temperatures (marks: experimental data; solid lines: theoretical model).

To complete the TFD electrical characterization, its incremental resistance is now considered. From the proposed model, we have

$$r_d = nV_T/(i_D + I_S) + \alpha R^{\alpha} i_D^{\alpha-1}. \tag{14}$$

The compound model makes a very good characterization of r_d for all operating temperature range. Only for very high currents, where the biochip will not operate, is the model not precise. At 1 μA and room temperature, $r_d \approx 0.2$ MΩ was obtained [6].

V. PIN Diode Modeling

The second TFD that has been considered for the biochip (from the technology available at INESC-MN) is a PIN diode due to some of its characteristics that may present advantages over Schottky-barrier diodes on the envisaged application [8].

PIN diode experimental characterization and data acquisition were performed using a specially designed and built controller, which allowed stabilization of the biochip temperature to a desired target. The DS600 analog temperature sensor (± 0.5 °C accuracy over -20 °C to $+100$ °C) [12] was integrated in the controller to measure in-site temperature. PIN diode experimental data (marks in Fig. 5) was collected for a temperature range between room temperature and 85 °C. TFD voltage was imposed over a -3 to 3 V range, and the corresponding diode current was measured and acquired with a picoammeter for ultralow current measurements.

For the PIN diode model derivation, three different operating regions (i.e., LCR, MCR, and HCR) were considered (LCR: $v_D < 0.5$ V; MCR: 0.5 V $< v_D <$ 2 V; and HCR: $v_D > 2$ V). As for the Schottky-barrier diode [see (11)], each established region model contributes with a term to the PIN diode voltage establishing the following compound model: $v_D = v_{J1} + v_{J2} + v_{\alpha}$ [7]. In the following sections, this complete compound model is derived as a step procedure, including the three defined current regions.

A. PIN Diode at Low Currents

The LCR I–V characteristics for positive voltages show that a straight-line approximation is possible but that the characteristics do not pass through the origin due to the influence of incident light present during experiments. An offset current I_0 (which disappears if there is no incident light) is then considered and is modeled as a current source in parallel with the diode. The PIN diode junction behavior in the LCR is then characterized by

$$v_{J1} = n_1 V_T \ln\left[1 + (i_D + I_0)/I_{S1}\right]. \tag{15}$$

From experimental data and this model, the following semi-empirical laws were derived for parameter dependence on temperature [7]:

$$\log\left[I_{S1}(T)\right] = k_{11} - k_{21}/T \tag{16}$$

$$n_1(T) = n_{11} + n_{21}T \quad I_0(T) = \beta + (\gamma T)^{\delta} \tag{17}$$

and obtained coefficients are $(I_{S1}[nA], I_0[nA], T[K])$: $k_{11} = 1.3826 \times 10^1$, $k_{21} = 5.3135 \times 10^3$, $n_{11} = 9.4766 \times 10^{-1}$, $n_{21} = 4.1857 \times 10^{-3}$, $\beta = 7.2071 \times 10^{-2}$, $\gamma = 2.6785 \times 10^{-3}$, and $\delta = 1.7577 \times 10^1$. This LCR model permits an excellent characterization for voltages over the -1 to $+0.75$ V range [7]. Although for our application, only PIN TFD direct operation is of concern, both direct and reverse operation regions are very well characterized by this LCR region. For higher voltages/currents (above 0.75 V), a second term must be considered, defining the MCR model.

B. PIN Diode at Medium Currents

For the MCR the Schockley equation is also used to model the second factor to describe the PIN diode behavior because its I–V characteristic suggests a typical diode response. The MCR model is then

$$v_D = v_{J1} + v_{J2} = v_{J1} + n_2 V_T \ln(1 + i_D/I_{S2}) \tag{18}$$

and $I_{S2}(T)$ and $n_2(T)$ are described by

$$\log\left[I_{S2}(T)\right] = k_{12} - k_{22}/T \quad n_2(T) = n_{12} + n_{22}/T \tag{19}$$

with $(I_{S2}[nA], T[K])$: $k_{12} = 7.9210$, $k_{22} = 1.7741 \times 10^3$, $n_{12} = 3.1787 \times 10^{-1}$, and $n_{22} = 1.5953 \times 10^3$ [7]. Abnormally high values for $n_2(T)$ were obtained, suggesting that although the PIN diode in the MCR is being modeled as a single diode, its behavior may correspond to the presence of more than one diode in series. Although the MCR was defined for 0.5 V $< v_D <$ 2 V, the MCR model achieves a very good match between the proposed model and the PIN diode experimental data for voltages until 2.25 V [7].

C. PIN Diode at High Currents

From the point of view of the developed microsystem, there is no need for HCR modeling because the maximum current allowed is limited by the MTJ. However, for the sake of completeness, an HCR model is derived based on the contribution of a nonlinear resistive term, as it has been considered for the

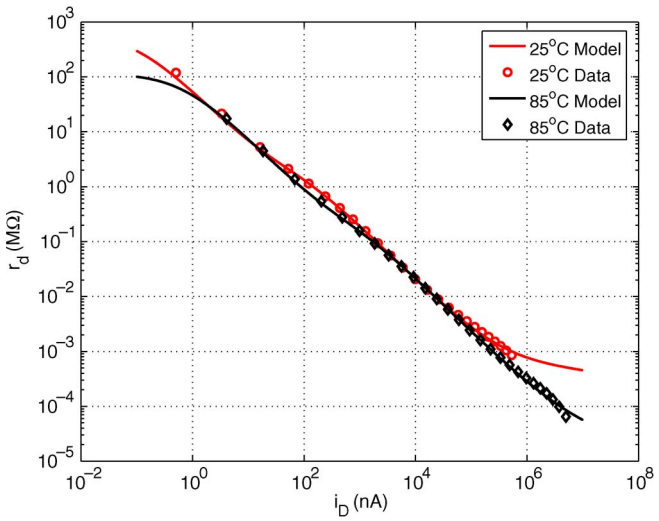

Fig. 6. PIN diode r_d at 25 °C and 85 °C (marks: experimental data; solid lines: theoretical model).

Schottky-barrier TFD (Section IV-B), defining the following complete compound model:

$$v_D = v_{J1} + v_{J2} + v_\alpha = v_{J1} + v_{J2} + (R\, i_D)^\alpha. \qquad (20)$$

Both parameters R and α have a temperature dependence described as follows:

$$\log\left[R(T)\right] = -r_1 + r_2/T \quad \alpha(T) = \alpha_1 - \alpha_2 T \qquad (21)$$

with coefficients $(R[\Omega], T[K])$: $r_1 = 4.5380$, $r_2 = 2.1803 \times 10^3$, $\alpha_1 = 1.6021$, and $\alpha_2 = 2.3974 \times 10^{-3}$ [7].

Fig. 5, besides depicting the PIN diode I–V experimental characterization (marks) at different temperatures, also shows the modeled PIN diode behavior (solid lines) obtained through the complete HCR compound model with all parameters' modeled temperature dependence with the estimated coefficients. It can be seen that the proposed model characterize PIN diodes very well over the entire forward operation voltage range.

For the PIN diode complete HCR model, the measured voltage sensitivity to the measuring current is modeled by

$$r_d = \frac{n_1 V_T}{i + I_0 + I_{S1}} + \frac{n_2 V_T}{i + I_{S2}} + \alpha R^\alpha i^{\alpha-1}. \qquad (22)$$

Both experimental data (marks) and the modeled r_d (solid lines) are depicted in Fig. 6. At room temperature and for a 1-μA driving current, $r_d \approx 0.2$ MΩ is obtained, which is a value similar to the one obtained for the Schottky-barrier diode.

Finally, PIN diode temperature sensitivity is considered. For the complete (HCR) compound model, the diode voltage sensitivity to temperature is $S_T^{v_D} = S_T^{v_{J1}} + S_T^{v_{J2}} + S_T^{v_\alpha}$, with

$$S_T^{v_{J1}} = \frac{K_B}{q}\left[\frac{n_1\delta(\gamma T)^\delta}{i + I_0} - k_{21}\ln(10)\frac{n_1}{T} - (n_{11} + 2n_{21}T)\ln\frac{I_{S1}}{i + I_0}\right] \qquad (23)$$

$$S_T^{v_{J2}} = -\frac{K_B}{q}\left[n_{12}\ln\frac{I_{S2}}{i} + k_{22}\ln(10)\frac{n_2}{T}\right] \qquad (24)$$

$$S_T^{v_\alpha} = -(Ri)^\alpha\left[r_2\ln(10)\frac{\alpha}{T^2} + \alpha_2\ln(Ri)\right]. \qquad (25)$$

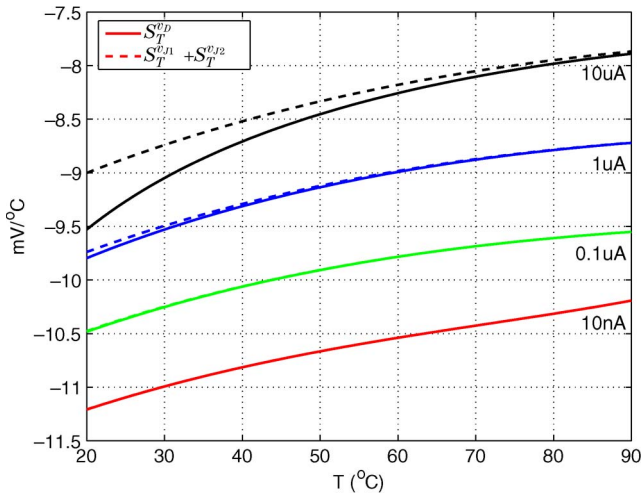

Fig. 7. PIN diode voltage sensitivity to temperature (solid lines: HCR model; dashed lines: MCR model) for several driving currents.

TABLE I
PIN AND SCHOTTKY-BARRIER DIODES' FORWARD AND REVERSE CURRENTS (+2.5 AND −2.5 V) AND ON/OFF RATIOS

	Forward	Reverse	On/off
Schottky-barrier	$60\,\mu A$	$-0.4\,\mu A$	1.3×10^5
PIN	$200\,\mu A$	$-0.12\,\mu A$	1.6×10^6

Fig. 7 shows for several driving current values the calculated sensitivities with the derived model. The complete compound model was considered (solid lines), and for comparison purposes, results for the intermediate MCR model (valid for the LCR and MCR) are also depicted (dashed lines). The $S_T^{v_D}$ variation with temperature does not show a perfect linear relation between the sensed voltage and the actual temperature value. It can be seen that nonlinearity is more pronounced for high current values, where the TFD is not expected to act as a temperature sensor. For this reason and because PIN diodes allow much higher current values than Schottky-barrier diodes, it is only necessary to consider the intermediate MCR model $S_T^{v_J1} + S_T^{v_J2}$ that is valid for $i_D < 100$ μA. It can be seen that temperature sensitivity is higher for lower driving currents and that sensitivities as high as -11 mV/°C may be achieved. To obtain more accurate temperature measurements, a calibration table, which is implemented on the onboard DSP, may be used to correct the displayed nonlinear behavior.

VI. PIN DIODE VERSUS SCHOTTKY-BARRIER DIODE

PIN diodes reveal some advantages over Schottky-barrier diodes that indicate that they may be more suitable for the biosensor included on our microsystem for biomolecular recognition detection. First, their on/off ratio is higher, as shown in Table I, for applied voltages of +2.5 and −2.5 V. The on/off ratio is important because it limits biochip size. Since both diodes have the same dimensions, PIN diode current density is higher, which allows smaller diodes to be made for the same current value. Schottky diodes have a maximum forward bias current at lower voltages than PIN diodes do, and if voltage increases, the diode may become irreversibly damaged. PIN diodes' higher conductance allows diode size reduction and MTJs to be used with a lower resistance and a larger area,

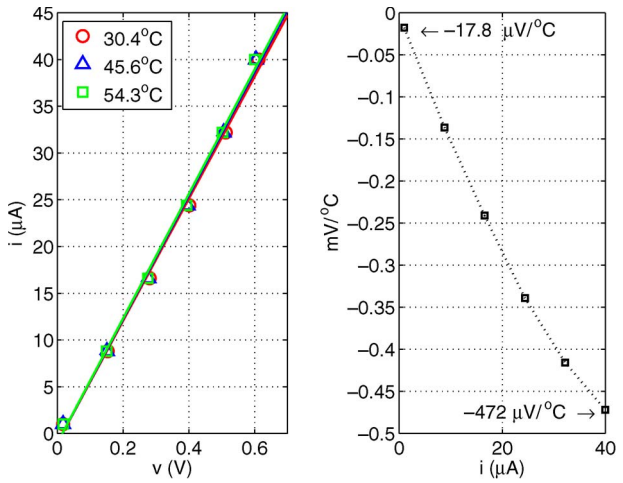

Fig. 8. (a) MTJ I–V (T) characteristics (marks: experimental data; solid lines: theoretical model). (b) MTJ $S_T^{v_S}$ measured with several driving currents.

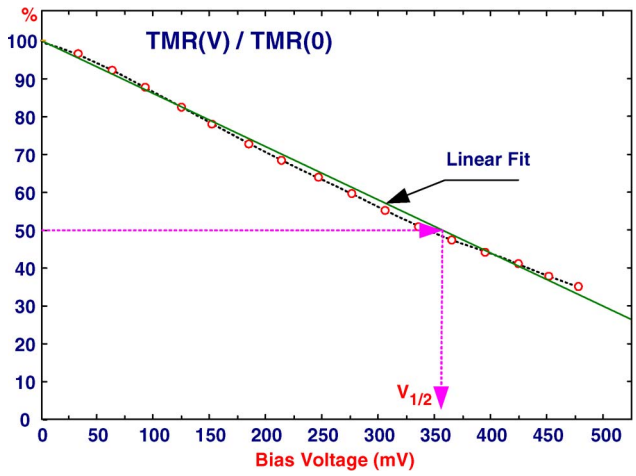

Fig. 9. MTJ TMR dependence on bias voltage (marks: experimental data; solid line: linear fit over data).

resulting in an increased dynamic range for the sensor (number of beads detected). A biochip with a matrix with an increased number of elements can then be developed. PIN diodes' temperature sensitivity is also higher (compare Figs. 3(b) and 7). For a driving current of 10 nA, Schottky diodes have a sensitivity of about -1.55 mV/°C and PIN diodes have a sensitivity of about -11 mV/°C, although nonlinearity correction may be needed. Finally, it can be stated that PIN diodes are also better behaved in the full current range in the sense that they fit the proposed theoretical model more accurately, particularly in the HCR. In addition, Schottky diodes do not present such a regular pattern on the I–V characteristics dependency on temperature as PIN diodes do (compare Figs. 4 and 5).

VII. MTJ Characterization and Modeling

A. MTJ Electrical and Temperature Characterization

Biochip MTJs have an I–V characteristic that may be very accurately modeled by a quadratic function. This parabolic shape may be envisaged in Fig. 8(a), where marks correspond to experimental data collected when the MTJ was driven by currents of $1-40$ μA at several operating temperatures (only three operating temperatures are shown). MTJ driving current was imposed, and its voltage was measured and digitally acquired through the average of ten measurements. Nevertheless, from a practical point of view, the MTJ I–V characteristic may be seen as having an almost linear characteristic, meaning it may be locally modeled by a straight line as follows:

$$i = i_0 + R_{\mathrm{MTJ}}^{-1} v \tag{26}$$

where $i_0 \neq 0$ indicates that the model only corresponds to a valid ohmic behavior in the vicinity of the measured data points. Experimental results showed that both parameters are temperature dependent and may be linearly modeled by

$$R_{\mathrm{MTJ}}(T) = R_x + \beta_x T, \qquad i_0(T) = i_x + \gamma_x T \tag{27}$$

with $R_x = 15.7$ kΩ, $\beta_x = -11.9$ Ω/°C, $i_x = -1.07$ μA, and $\gamma_x = 0.98$ nA/°C [6]. Solid lines in Fig. 8(a) show the obtained results with these models. Their good match with experimental data [marks in Fig. 8(a)] assures that the proposed linear models may be used for MTJ electrical and temperature characterization. Due to the ultralow thickness of the dielectric needed to obtain a tunneling effect, typical MTJs may break down for applied voltages over 1.1 V. This limits the maximum secure driving current at room temperature to ≈70 μA for a biochip with a nominal $R_{\mathrm{MTJ}} = 15.3$ kΩ [6].

MTJ $S_T^{v_S}$ may be determined from the proposed linear models [solid lines in Fig. 8(b)], and for a driving current of 1 μA, a -17.8 μV/°C sensitivity is obtained [6]. This value is negligible when compared with $S_T^{v_D}$ exhibited by both diodes that are in series with the MTJ on each biosensor matrix node. Both considered TFDs may then be used as local temperature sensors because MTJs very low temperature sensitivity is imperceptible.

B. MTJ Magnetic Characterization

MTJ resistance varies with the transversal component of an applied magnetic field, and its sensitivity is measured by the tunneling magnetoresistance ratio TMR. A maximum variation occurs when no voltage is applied to the MTJ, i.e.,

$$TMR(0) = [(R_{\max} - R_{\min})/R_{\min}] \times 100\% \tag{28}$$

where $R_{\max}$ and $R_{\min}$ are the maximum and minimum values obtained with magnetic opposite saturation fields (typically ± 10 Oe, $\Delta H_{\max}$). For the considered MTJ, TMR is almost constant until 30 mV ($TMR(0) \cong 27\%$—see TMR subfigure inside Fig. 10) and then decreases almost linearly with an increase in bias voltage. Inside the 300–500 mV range, where TMR drops to half its initial value, i.e., $V_{1/2}$, the following model is possible (see Fig. 9):

$$TMR(V) = TMR(0)\left[1 - V/(2V_{1/2})\right] \tag{29}$$

showing MTJ TMR dependence on the applied dc bias voltage. However, a bias voltage reduction implies a driving current reduction, which increases r_d, reducing the reading voltage v_M (Fig. 2). Driving current optimization is then needed to maximize v_M.

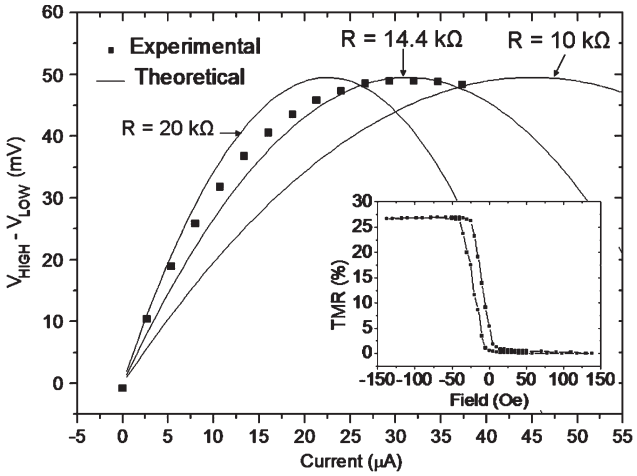

Fig. 10. MTJ voltage variation dependence with the driving current (marks: experimental data; solid lines: theoretical model).

Although TMR decreases with an increase in bias voltage, if a very small current is applied to the MTJ to have full TMR, MTJ voltage will also be very small, and the voltage variation ΔV (voltage at high MTJ resistance minus voltage at low MTJ resistance) will also be very low. This means that there is a tradeoff between these two phenomena, and that $\Delta V_{\max}$ is observed at a certain current value. This current depends on the MTJ resistance: the higher the resistance is, the lower the current at which the maximum is observed will be (solid lines in Fig. 10). Its value may be derived, taking into account that

$$S_H^{v_S} = S_H^{R_S} \times i_M, \qquad S_H^{R_S} = TMR(V) \times R_S / \Delta H_{\max} \tag{30}$$

and may be estimated as $V_{1/2}/R_S$. Experimental characterization of one of the biochip MTJs showed a resistance of 14.4 kΩ, and $\Delta V_{\max}$ occurs for a driving current of ≈ 30 μA (square marks in Fig. 10). Device simulations for three different MTJ resistances are also shown as solid lines and agree well with experimental data. All curves show a maximum $\Delta V \approx 50$ mV. The decrease of ΔV for higher bias currents is caused by TMR decrease at increasing bias voltage. For our biochip application, a maximum voltage variation is required. Increasing MTJ resistance decreases the current required to maximize signal output, but at the expense of increased sensor noise (mostly $1/f$ for low-frequency applications). On the other hand, lowering MTJ resistance pushes the maximum signal peak to higher currents.

A magnetoresistive biochip with a matrix structure based on the TFD-MTJ series has already been tested for biomolecular detection [8]. When a magnetically labeled DNA strand is recognized, a voltage variation occurs. Nevertheless, as shown in this article, a voltage variation can also occur due to temperature variation. Thus, the proposed temperature model of the device is of great importance to distinguish temperature variations from magnetic particle detection. Preliminary results show that the Schottky-MTJ basic cell has a higher ability to detect a lower number of particles than the PIN-MTJ, improving individual particle sensitivity. For 100 nm, the Schottky-MTJ sensor is capable of detecting down to 7 particles, while the PIN-MTJ only distinguishes 21 particles. For 50 nm, 20 particles are detected by the Schottky-MTJ, while the PIN-MTJ only identifies 100 particles [8].

VIII. Conclusion

Electrical, temperature, and magnetic modeling and experimental characterization of Schottky-barrier and PIN TFDs and MTJs, included on a magnetoresistive biochip based on a 16 × 16 scalable matrix structure, were performed in this work. The fabricated biochip was integrated on a portable handheld microsystem for biomolecular recognition detection using magnetic labels. Schottky-barrier and PIN diodes were considered as the switching devices for matrix row–column connection as well as an accurate temperature sensor for local temperature sensing and system calibration. PIN diodes have better characteristics for the envisaged application (support higher currents and have higher on/off ratio and higher temperature sensitivity) mainly because their properties may lead to biochip size reduction. On the other hand, Schottky-barrier diodes have shown an almost linear voltage sensitivity to temperature, which may simplify nonlinearity compensation procedures needed for PIN diodes' accurate temperature measurements. MTJs' temperature sensitivity may be disregarded because it is much lower than those of both TFD types and its electric and magnetic sensitivities are linear on the handheld operating conditions. The biosensor proposed models for both TFDs and the MTJ and their parameter estimation has proven to characterize biosensors behavior very well, which means that they can be considered for biochip characterization and system calibration. Provided results indicate that the diode may be used both as the matrix switching device and as an in-site temperature sensor and that the MTJ may act as the magnetoresistive sensor, detecting the fringe field of immobilized magnetic markers. The fabricated fully integrated biochip included in the developed handheld microsystem may then be used for biomolecular recognition.

References

[1] H. A. Ferreira, D. L. Graham, P. P. Freitas, and J. M. S. Cabral, "Biodetection using magnetically labelled biomolecules and arrays of spin valve sensors," *J. Appl. Phys.*, vol. 93, no. 10, pp. 7281–7286, May 2003.

[2] W. Shen, X. Liu, D. Mazumdar, and G. Xiao, "In situ detection of single micron-sized magnetic beads using magnetic tunnel junction sensors," *Appl. Phys. Lett.*, vol. 86, no. 25, p. 253 901, Jun. 2005.

[3] J. Germano, M. S. Piedade, L. Sousa, T. M. Almeida, P. Lopes, F. A. Cardoso, H. A. Ferreira, and P. P. Freitas, "Microsystem for biological analysis based on magnetoresistive sensing," presented at the XVIII IMEKO World Congr., Rio de Janeiro, Brazil, Sep. 2006, Paper 00286. CD Proceedings.

[4] M. S. Piedade, L. Sousa, T. M. de Almeida, J. Germano, B. A. da Costa, J. M. Lemos, P. P. Freitas, H. A. Ferreira, and F. Cardoso, "A new hand-held microsystem architecture for biological analysis," *IEEE Trans. Circuits Syst. I, Reg. Papers*, vol. 53, no. 11, pp. 2384–2395, Nov. 2006.

[5] L. Sousa, M. S. Piedade, J. Germano, T. M. de Almeida, P. A. C. Lopes, F. Cardoso, and P. Freitas, "Generic architecture designed for biomedical embedded systems," in *Embedded System Design: Topics, Techniques and Trends*, A. Rettberg, M. C. Zanella, R. Domer, A. Gerstlauer, and F. J. Ramming, Eds. New York: Springer-Verlag, Apr. 2007, pp. 353–362.

[6] T. M. Almeida, M. S. Piedade, F. Cardoso, H. A. Ferreira, and P. P. Freitas, "Characterisation and modelling of a magnetic biosensor," in *Proc. IEEE IMTC*, Sorrento, Italy, Apr. 2006, pp. 2007–2012.

[7] T. M. Almeida, M. S. Piedade, P. C. Lopes, L. Sousa, J. Germano, F. Cardoso, H. A. Ferreira, and P. P. Freitas, "Magnetoresistive biosensor modelling for biomolecular recognition," presented at the XVIII IMEKO World Congr., Rio de Janeiro, Brazil, Sep. 2006, Paper no. 00386. CD Proceedings.

[8] F. Cardoso, R. Ferreira, S. Cardoso, J. Conde, V. Chu, P. Freitas, J. Germano, T. M. de Almeida, L. Sousa, and M. S. Piedade, "Noise characteristics and particle detection limits in diode + MTJ matrix elements for biochip applications," *IEEE Trans. Magn.*, vol. 43, no. 6, pp. 2403–2405, May 2007.
[9] S. M. Sze, *Physics of Semiconductor Devices*. Hoboken, NJ: Wiley, 1981.
[10] L. F. Marsal, J. Pallares, X. Correig, J. Calderer, and R. Alcubilla, "Electrical model for amorphous/crystalline heterojunction silicon diodes (n a-Si:H/p c-Si)," *Semicond. Sci. Technol.*, vol. 10, no. 8, pp. 1209–1213, Aug. 1996.
[11] D. A. Hodges and H. G. Jackson, *Analysis and Design of Digital Integrated Circuits*, 2 ed. New York: McGraw-Hill, 1988.
[12] Maxim-Dallas Semiconductor, *DS600 $\pm 0:5\ ^{\circ}C$ Accurate Analog-Output Temperature Sensor*, 2004. rev. 082505. [Online]. Available: www.maxim-ic.com

Teresa Mendes de Almeida received the licentiate degree, M.Sc., and Ph.D. degrees in electrical and computer engineering from the Technical University of Lisbon, Lisbon, Portugal, in 1988, 1994, and 2005, respectively.

She is a Professor with the Department of Electrical and Computers Engineering, Instituto Superior Técnico (IST), Technical University of Lisbon, and a Researcher with the Instituto de Engenharia de Sistemas e Computadores-R&D (INESC-ID), Lisbon. Her research interests include analog and digital PLLs, signal acquisition and processing systems, DSP algorithms, and system modeling.

Moisés S. Piedade received the Ph.D. degree in electrical and computer engineering from the Technical University of Lisbon, Lisbon, Portugal, in 1983.

He is a Professor with the Department of Electrical and Computer Engineering, Instituto Superior Técnico (IST), Technical University of Lisbon, and the Leader of Signal Processing Systems Research Group, Instituto de Engenharia de Sistemas e Computadores-R&D (INESC-ID), Lisbon. His main research interests include electronic systems, signal acquisition and processing systems and circuits, and systems for biomedical applications.

Leonel Augusto Sousa (M'01–SM'03) received the licentiate degree in electronic and telecommunications engineering from the Universidade de Aveiro, Aveiro, Portugal, in 1984, and the M.Sc. and Ph.D. degrees in electrical and computer engineering from the Technical University of Lisbon, Lisbon, Portugal, in 1989 and 1996, respectively.

He is currently an Associate Professor with the Department of Electrical and Computer Engineering, Instituto Superior Técnico (IST), Technical University of Lisbon, and a Senior Researcher with the Instituto de Engenharia de Sistemas e Computadores-R&D (INESC-ID), Lisbon. His research interests include computer architectures, parallel and distributed computing, and VLSI architectures for multimedia and biomedical systems. He is the author of more than 150 papers published in international journals and conferences.

Dr. Sousa is a member of the IEEE Computer Society, a member of the Association for Computing Machinery, and a member of the European Network of Excellence on High Performance and Embedded Architecture and Compilation (HiPEAC).

José Germano received the licentiate degree in electrical and computer engineering and the M.Sc. degree in 2004 and 2006, respectively, from the Technical University of Lisbon, Lisbon, Portugal, where he is currently working toward the Ph.D. degree. His doctoral study focuses on the improvement of a data acquisition and processing platform for DNA recognition using a magnetoresistive biochip.

His research interests include bioelectronics/biomedical instrumentation implantable and wearable electronics and processor microarchitectures.

Paulo A. C. Lopes received the Ph.D. degree in electrical and computer engineering from the Technical University of Lisbon, Lisbon, Portugal, in 2004.

He is an Auxiliary Professor with the Department of Electrical and Computer Engineering, Instituto Superior Técnico (IST), Technical University of Lisbon, and a Researcher with the Signal Processing Systems Research Group, Instituto de Engenharia de Sistemas e Computadores-R&D (INESC-ID), Lisbon. His main research interests include digital signal processing for acoustics, telecommunications, biomedical applications, and bioinformatics.

Filipe Arroyo Cardoso received the licentiate degree in physics engineering from the Technical University of Lisbon, Lisbon, Portugal, where he is currently working toward the Ph.D. degree at the Instituto Superior Técnico (IST).

He is also with the Instituto de Engenharia de Sistemas e Computadores-Microsistemas and Nanotecnologias (INESC-MN), Lisbon, Portugal, working on magnetoresistive biochips.

Paulo Peixeiro Freitas (M'90) received the Ph.D. degree in solid-state physics from Carnegie Mellon University, Pittsburgh, PA, in 1986.

He is currently a Full Professor with the Department of Physics, Instituto Superior Técnico (IST), Technical University of Lisbon, Lisbon, Portugal, and the Director of the Instituto de Engenharia de Sistemas e Computadores-Microsistemas and Nanotecnologias (INESC-MN), Lisbon. His current research interests include MRAMS, read heads for ultra-high-density recording, magnetoresistive biochips, and sensors for biomedical applications.